# Validation of NO2 and HNO3 measurements from the Improved Limb Atmospheric Spectrometer (ILAS) with the version 5.20 retrieval algorithm

H. Irie, Y. Kondo, M. Koike, M. Danilin, Claude Camy-Peyret, Sébastien Payan, Jean-Pierre Pommereau, Florence Goutail, H. Oelhaf, G. Wetzel, et al.

# Validation of $NO_2$ and $HNO_3$ measurements from the Improved Limb Atmospheric Spectrometer (ILAS) with the version 5.20 retrieval algorithm

H. Irie,[1] Y. Kondo,[2] M. Koike,[3] M. Y. Danilin,[4] C. Camy-Peyret,[5] S. Payan,[5] J. P. Pommereau,[6] F. Goutail,[6] H. Oelhaf,[7] G. Wetzel,[7] G. C. Toon,[8] B. Sen,[8] R. M. Bevilacqua,[9] J. M. Russell III,[10] J. B. Renard,[11] H. Kanzawa,[12] H. Nakajima,[12] T. Yokota,[12] T. Sugita,[12] and Y. Sasano[12]

Received 30 August 2001; revised 9 January 2002; accepted 18 January 2002; published 20 September 2002.

[1] The Improved Limb Atmospheric Spectrometer (ILAS) on board the Advanced Earth Observing Satellite (ADEOS) measured nitrogen dioxide ($NO_2$) and nitric acid ($HNO_3$) profiles from November 1996 to June 1997 at high latitudes in both hemispheres. The ILAS $NO_2$ profiles (version 5.20) are compared with those obtained by balloon-borne and satellite measurements to validate ILAS $NO_2$ data. Comparisons with balloon-borne measurements indicate that ILAS $NO_2$ at 25–30 km has a positive bias of 0.3–0.4 ppbv (6–11%). The random difference in $NO_2$ at 25–30 km is 0.2–0.3 ppbv (3–9%). The random error in the ILAS $NO_2$ measurements is larger than 100% below 20 km and above 45 km, where the $NO_2$ mixing ratios were less than 1.0 ppbv. It is possible that ILAS $NO_2$ values were lowered by optically thick aerosols with aerosol extinction coefficients at 780 nm of greater than 0.001 $km^{-1}$. The lack of diurnal correction along the line of sight contributes to the positive bias in the ILAS $NO_2$ values below 25 km. Agreement of the ILAS $NO_2$ values with those by the Polar Ozone and Aerosol Measurement (POAM) II instrument is within 10–30% at 25–35 km. The agreement with the Halogen Occultation Experiment (HALOE) is as good as ±10% at 25–40 km. ILAS $HNO_3$ (version 5.20) agrees with balloon-borne $HNO_3$ to within 0.1 ppbv (0–1%), and the random difference is within 10% at 25–30 km. *INDEX TERMS:* 0340 Atmospheric Composition and Structure: Middle atmosphere—composition and chemistry; 0341 Atmospheric Composition and Structure: Middle atmosphere—constituent transport and chemistry (3334); 0394 Atmospheric Composition and Structure: Instruments and techniques

**Citation:** Irie, H., et al., Validation of $NO_2$ and $HNO_3$ measurements from the Improved Limb Atmospheric Spectrometer (ILAS) with the version 5.20 retrieval algorithm, *J. Geophys. Res.*, *107*(D24), 8206, doi:10.1029/2001JD001304, 2002.

[1]Solar-Terrestrial Environment Laboratory, Nagoya University, Aichi, Japan.
[2]Research Center for Advanced Science and Technology, University of Tokyo, Tokyo, Japan.
[3]Department of Earth and Planetary Science, Graduate School of Science, University of Tokyo, Tokyo, Japan.
[4]Atmospheric and Environmental Research, Inc., Lexington, Massachusetts, USA.
[5]Laboratoire de Physique Moléculaire et Applications, Université Pierre et Marie Curie, CNRS, Paris, France.
[6]Service d'Aéronomie du CNRS, Verrières le Buisson, France.
[7]Institut für Meteorologie und Klimaforschung, Forschungszentrum Karlsruhe, Karlsruhe, Germany.
[8]Jet Propulsion Laboratory, California Institute of Technology, Pasadena, California, USA.
[9]Naval Research Laboratory, Washington, District of Columbia, USA.
[10]Atmospheric Science Division, NASA, LaRC, Hampton, Virginia, USA.
[11]Laboratoire de Physique et Chimie de l'Environnement, CNRS, Orléans, France.
[12]National Institute for Environmental Studies, Tsukuba, Japan.


0148-0227/02/2001JD001304

## 1. Introduction

[2] It is well known that $NO_x$ (= NO + $NO_2$) destroys stratospheric ozone via the following catalytic cycle [*Crutzen*, 1970]:

$$\text{(R1)} \qquad NO + O_3 \rightarrow NO_2 + O_2$$

$$\text{(R2)} \qquad NO_2 + O \rightarrow NO + O_2$$

$$\text{(R3)} \qquad \text{Net}: \; O + O_3 \rightarrow 2O_2$$

The $NO_x$ catalytic cycle is the dominant mechanism of ozone loss in the middle stratosphere [*Jucks et al.*, 1996; *Osterman et al.*, 1997] and also in the lower stratosphere during polar summer [*Fahey et al.*, 2000]. In addition, $NO_2$ regulates the stratospheric ozone budget via reactions with radicals (ClO, BrO, OH, and $NO_3$) to form reservoir species ($ClONO_2$, $BrONO_2$, $HNO_3$, and $N_2O_5$). Therefore, the

**Table 1.** List of Balloon Experiments

| Experiment | Date | Location at 20 km | SZA | Distance,[a] km | Time Difference,[a] hours |
|---|---|---|---|---|---|
| LPMA | Feb. 26 | 66.9°N, 20.5°E | ~90° | 570 | 0.6 |
| SAOZ | Feb. 24 | 67.4°N, 19.2°E | ~90° | 1010 | 1.8 |
| SAOZ | March 20 | 66.9°N, 17.6°E | ~90° | 620 | 0.9 |
| MIPAS-B2 | March 24 | 69.6°N, 30.1°E | ~105° | 200 | 3.6 |
| MkIV | May 8 | 68.6°N, 146.3°W | ~90°[b] | 760 | 6.4 |

[a] Values between the ILAS and balloon-borne measurement locations.
[b] MkIV measurement was made in the morning, whereas the ILAS measurement was made in the evening.

observation of $NO_2$ in the stratosphere is important in studies regarding ozone depletion.

[3] The Improved Limb Atmospheric Spectrometer (ILAS) on board the Advanced Earth Observing Satellite (ADEOS) is a solar occultation sensor. ILAS measured concentrations of atmospheric constituents including $NO_2$ in the stratosphere at high latitudes in the Northern Hemisphere (NH) and Southern Hemisphere (SH) from November 1996 through June 1997. A balloon-borne measurement campaign for the validation of ILAS data was conducted at Kiruna, Sweden (68°N, 21°E) in February and March 1997, and Fairbanks, Alaska (65°N, 148°W) in May 1997 [*Kanzawa et al.*, 1997]. Vertical profiles of $NO_2$ were obtained during this campaign.

[4] In the present paper, $NO_2$ profiles obtained by ILAS are compared with those obtained by several balloon-borne and satellite measurements, and the quality of ILAS $NO_2$ retrieved using the version 5.20 algorithm is described. Because of diurnal variations in $NO_2$ concentration, the comparisons are made under similar instantaneous sunlight conditions. To minimize the effect of the differences in the measurement locations, the comparisons of $NO_2$ for winter and early spring are made only when the ILAS and correlative measurements were made at similar potential vorticity (PV) values. To make consistent evaluations of ILAS reactive nitrogen measurements, similarly to $NO_2$, the quality of version 5.20 ILAS $HNO_3$ measurements is briefly reported in the appendix, while *Koike et al.* [2000] have already reported the quality of version 3.10 ILAS $HNO_3$ data.

## 2. ILAS

[5] The ADEOS satellite carrying ILAS was launched into a 98.6°-inclination Sun-synchronous polar orbit, resulting in 14 ILAS measurements in each hemisphere per day. Routine ILAS measurements at sunset (SS) were performed from November 1996 to June 1997 in NH, and from November 1996 to March 1997 in SH, and at sunrise (SR) from April to June 1997 in SH [*Sasano et al.*, 1999a], with some measurements in September and October 1996. The latitudes of 57°–72°N and 64°–89°S were covered during these periods. The solar zenith angle (SZA) of the measurements was 90.2 ± 0.2° at 20–50 km. The horizontal width of the ILAS sampling volume is calculated to be 13 km from its field of view. Air density-weighted absorption of solar radiation occurred over an effective path length of about 220 km. Vertical resolutions estimated from the instantaneous field of view are 1.9, 2.5, 3.0, and 3.5 km at altitudes of 15, 25, 35, and 55 km, respectively [*Yokota et al.*, 2002]. The $NO_2$ mixing ratio was retrieved up to 50 km every 1 km using an onion-peeling method [*Yokota et al.*, 2002]. $NO_2$ absorption at wavelengths between 6.2 and 6.3 μm was measured by ILAS.

[6] The sum of the systematic and random errors in retrieving $NO_2$ mixing ratios with the version 5.20 algorithm was estimated primarily from the errors in the spectral fitting and atmospheric temperature. The percentage value is about 20% at 30 km and becomes progressively larger at higher and lower altitudes [*Yokota et al.*, 2002]. Multiplying by the average of all $NO_2$ profiles measured by ILAS, the absolute values of the errors at 15–30 km and 30–50 km are calculated to be 0.5–1.5 and 1.5–2.5 ppbv, respectively. The systematic error of ILAS $NO_2$ data will be estimated from the comparisons with balloon-borne measurements in the present study.

## 3. Comparisons With Balloon-Borne Measurements

### 3.1. Approach

[7] The balloon-borne measurements used in this study are summarized in Table 1. The ILAS $NO_2$ measurements are compared with 4 balloon-borne measurements in 1997 (5 $NO_2$ profiles): (1) the Limb Profile Monitor of the Atmosphere (LPMA) measurement performed on 26 February, (2) the balloon-borne Système d'Analyze d'Observations Zénithales (SAOZ) measurements performed on 24 February and 20 March, (3) the Michelson Interferometer for Passive Atmospheric Sounding-Balloon-borne version 2 (MIPAS-B2) measurement performed on 24 March, and (4) the MkIV measurement performed on 8 May. These measurements in the validation campaign acquired $NO_2$ profiles on the same UT days as the ILAS measurements and at locations within ~1000 km distance of ILAS measurement points. A coincidence criterion in PV was taken as within ±10% of the PV at the ILAS measurements. Applying this PV criterion to the measurement points for each altitude, the altitude levels at which the difference in PV for the balloon and ILAS measurements

**Table 2.** Performance of the Balloon-Borne Measurements at 25 km

| Experiment | Vertical Resolution,[a] km | Precision,[b] % | Accuracy,[b] % |
|---|---|---|---|
| LPMA | 1.5 | 10 | 15 |
| SAOZ | 1.2 | 8 | 13 |
| MIPAS-B2 | 1.2 | 11 | 15 |
| MkIV | 1.5 | 4 | 8 |

[a] Estimated from the instantaneous field of view.
[b] One-σ values of the volume mixing ratios.

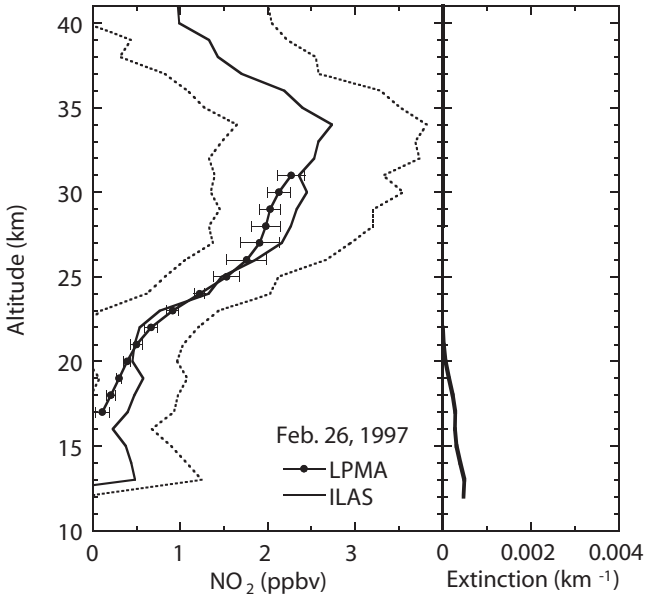


**Figure 1.** Comparison of ILAS with LPMA $NO_2$ measurements on 26 February 1997. Left panel: Thick line indicates the ILAS $NO_2$ profile. Dashed lines indicate the error of the ILAS $NO_2$ measurements. The balloon-borne $NO_2$ profile at SS is shown by the line with solid symbols. Associated bars indicate the error of the balloon-borne measurements. Right panel: Profile of the ILAS aerosol extinction coefficient at 780 nm.

was larger than 10% were rejected. Since the PV differences between equatorward and poleward edges of the Arctic vortex boundary region were usually about 20–30% in NH during the winter considered here [e.g., *Koike et al.*, 2000], this criterion is narrow enough to exclude the comparison of air masses having different characteristics, such as between air masses inside and outside the vortex. To make comparisons under the same SZA conditions with distinction of SS and SR as the ILAS measurements, MIPAS-B2 and MkIV profiles were diurnally corrected by a model calculation as described in sections 3.2.3 and 3.2.4, respectively.

[8] Heterogeneous reactions on the surface of polar stratospheric cloud (PSC) particles convert $NO_2$ to $HNO_3$, lowering the $NO_2$ concentration. Air masses sampled by balloon-borne instruments and ILAS were sometimes colder than the nitric acid trihydrate condensation temperature ($T_{NAT}$). The effect of heterogeneous reactions has been assessed by the period when these air masses were cooled to below $T_{NAT}$. Using the European Centre for Medium-Range Weather Forecasts (ECMWF) wind and temperature fields, 10-day isentropic back trajectories of air masses at ILAS and balloon-borne measurement points were calculated. $T_{NAT}$ was calculated following the method described by *Hanson and Mauersberger* [1988].

[9] For all comparisons except for SAOZ on 24 February, the balloon-borne and ILAS air masses experienced temperatures below $T_{NAT}$ for periods as short as 0–1 day. Air masses sampled by ILAS at 16–24 km and SAOZ at 15–23 km on 24 February experienced temperatures below $T_{NAT}$ for 43 hours over 10 days, suggesting similar reductions in $NO_2$ concentrations by heterogeneous reactions on PSCs for ILAS and SAOZ measurements. Therefore, the present study does not make any corrections for heterogeneous reactions on PSCs.

[10] The ILAS $NO_2$ mixing ratios used for the comparison were linearly interpolated to the potential temperature levels corresponding to altitudes at which balloon-borne measurements were made. The United Kingdom Meteorological Office (UKMO) pressure and temperature were used for this calculation.

### 3.2. $NO_2$ Profiling by Balloon-Borne Measurements

#### 3.2.1. LPMA

[11] The LPMA instrument developed at Laboratoire de Physique Moléculaire et Applications is a Fourier transform infrared (FTIR) spectrometer that measures the vertical profiles of various species from solar occultation spectra [*Camy-Peyret*, 1995]. The LPMA $NO_2$ vertical profile measurement was performed on 26 February 1997 near Kiruna, Sweden, during SS (SZA ~90°). The 170 spectra recorded during the flight showed sufficient absorption by $NO_2$ molecules for the precise retrieval in the appropriate microwindow around 3.4 μm (2915 $cm^{-1}$). A global fit algorithm associated with an efficient minimization algorithm of the Levenberg-Marquardt type allows the retrieval of vertical profiles of $NO_2$ from the occultation spectra [*Payan et al.*, 1998].

#### 3.2.2. SAOZ

[12] The SAOZ sonde is a UV-visible diode array spectrometer derived from the ground-based SAOZ designed for the monitoring of ozone and $NO_2$ total columns [*Pommereau and Goutail*, 1988]. SAOZ $NO_2$ vertical profile measurements were performed on 24 February and 20 March 1997 from Kiruna, Sweden, during SS (SZA ~90°). $NO_2$ was measured by differential spectroscopy over a large spectral range of 410–530 nm using the absorption cross sections at 220 K of *Vandaele et al.*

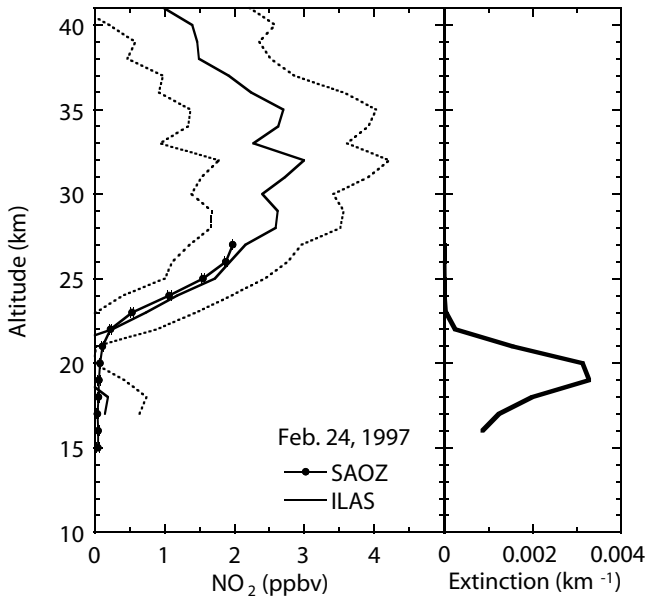


**Figure 2.** Same as Figure 1, but for the comparison with the SAOZ $NO_2$ measurements on 24 February 1997.

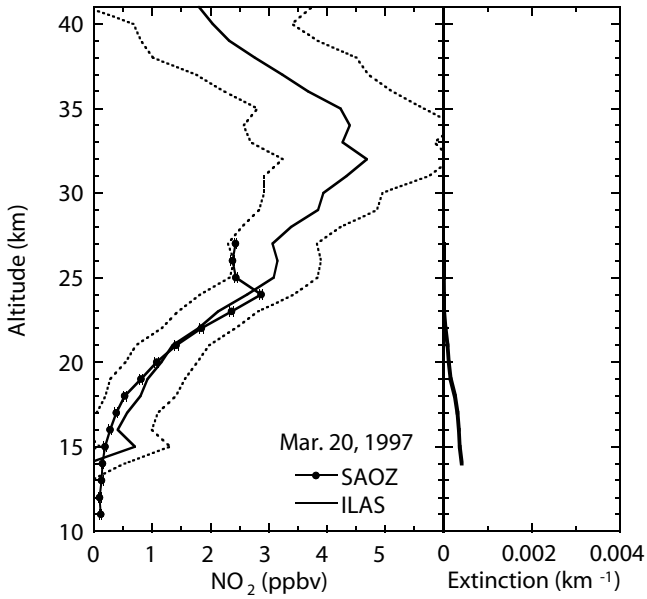


**Figure 3.** Same as Figure 1, but for the comparison with the SAOZ $NO_2$ measurements on 20 March 1997.

[1998]. Concentration profiles were retrieved by a linear tangent ray inversion technique (onion peeling).

### 3.2.3. MIPAS-B2

[13] The MIPAS-B2 instrument is a cryogenic FTIR spectrometer that measures atmospheric thermal emissions from the limb [*Oelhaf et al.*, 1996; *Friedl-Vallon et al.*, 1999]. The MIPAS-B2 $NO_2$ vertical profile measurement was performed on 24 March 1997 near Kiruna, Sweden, during the nighttime (SZA $\sim$105° at 20 km). $NO_2$ was measured using the $\nu_3$ band between 6.2 and 6.3 μm (1585 and 1615 $cm^{-1}$). The vertical profile of $NO_2$ mixing ratios was retrieved by an onion-peeling technique and a multiparameter nonlinear least squares fitting procedure [*Wetzel et al.*, 2002].

[14] The 3-dimensional Karlsruhe Simulation Model of the Middle Atmosphere (KASIMA) [*Ruhnke et al.*, 1999] was used to convert the nighttime $NO_2$ values to those at SS at the ILAS measurement point, by multiplying the MIPAS $NO_2$ values with the ratio of the model $NO_2$ values for the time and location of ILAS and MIPAS-B2 measurements. The model uses the 6-hourly analyses of the ECMWF wind and temperature data that are dynamically interpolated in space and time to the model environment up to a pressure level of 10 hPa [*Reddmann et al.*, 2001]. The model was initialized on 10 December 1996 using data from a 2-dimentional model (for details, see *Wetzel et al.* [2002]). The chemistry module consists of 58 chemical species and families, which are involved in 101 gas-phase reactions, 39 photodissociation reactions, and 10 heterogeneous reactions taking place on the surface of polar stratospheric clouds and liquid sulfuric acid aerosols. The rate constants of the gas phase reactions and the surface reaction probabilities are taken from the compilation of *DeMore et al.* [1997] with the update of *Sander et al.* [2000].

### 3.2.4. MkIV

[15] The MkIV instrument, which is a solar occultation FTIR spectrometer, measures the concentrations of various chemical species simultaneously [*Toon*, 1991; *Sen et al.*, 1998]. The MkIV $NO_2$ vertical profile measurement was performed on 8 May 1997 from Fairbanks, Alaska, during SR (SZA $\sim$90°), where the ILAS measurement in NH was made during SS. $NO_2$ was measured using the wavelengths of 6.1–6.3 and 3.4–3.5 μm. From a series of spectra measured at different tangent altitudes, the vertical profiles of chemical species were retrieved.

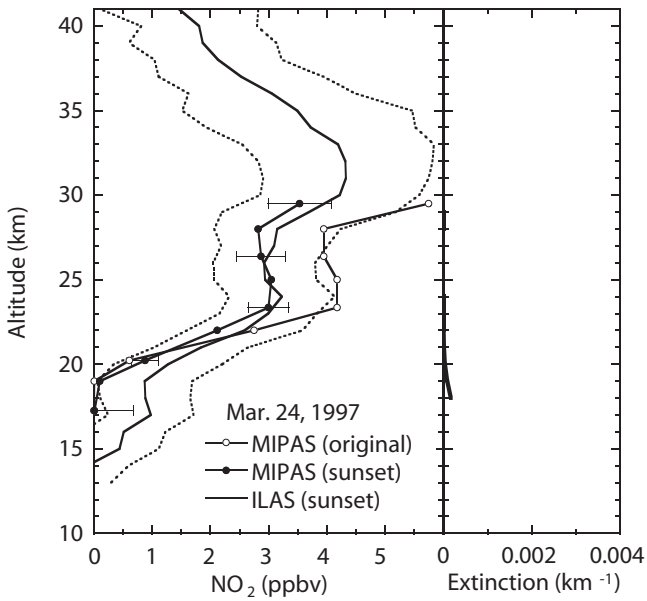


**Figure 4.** Same as Figure 1, but for the comparison with the MIPAS-B2 $NO_2$ measurements on 24 March 1997. The original balloon-borne $NO_2$ profile (SZA $\sim$105°) is shown by the line with open symbols for reference.

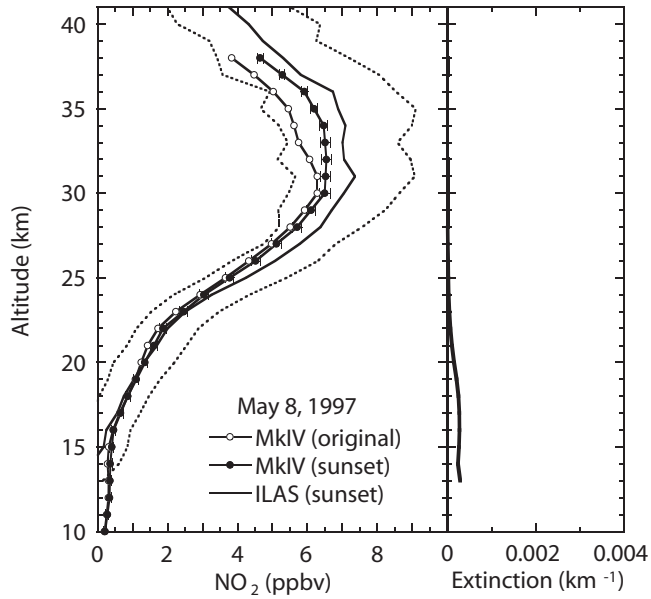


**Figure 5.** Same as Figure 1, but for the comparison with the MkIV $NO_2$ measurements on 8 May 1997. The original balloon-borne $NO_2$ profile (SZA $\sim$90° in the morning) is shown by the line with open symbols for reference.

**Table 3.** Altitudes Used for the Comparison and Altitudes Where the $|\Delta NO_2|$ Value Was Greater Than 0.5 ppbv

| Experiment | Date | Altitudes for Comparison | $\|\Delta NO_2\| > 0.5$ ppbv |
|---|---|---|---|
| LPMA | Feb. 26 | 17–19 km (boundary)<br>24–31 km (inside) | – |
| SAOZ | Feb. 24 | 16–27 km (inside) | 19–21 km (ILAS low) |
| SAOZ | March 20 | 14–26 km (boundary) | 25–26 km (ILAS high) |
| MIPAS-B2 | March 24 | 18–29 km (inside) | 18–20 km (ILAS high) |
| MkIV | May 8 | 15–38 km (outside) | 25–37 km (ILAS high) |

Altitudes used for the comparison have been chosen with PV differences less than 10%. Measurements in the vortex boundary and inside and outside the vortex are denoted by "boundary," "inside," and "outside," respectively.

[16] A photochemical model [*Osterman et al.*, 1999, and references therein] was used to convert $NO_2$ values at SR to those at SS. The model is constrained by temperature, pressure, $O_3$, $H_2O$, $CH_4$, CO, $NO_y$, and $Cl_y$, inferred from MkIV measurements. The input $O_3$ and temperature profiles are taken from the measurements, including MkIV [*Sen et al.*, 1998]. The abundance of radical (e.g., NO, $NO_2$) and reservoir (e.g., $HNO_3$, $N_2O_5$) gases were calculated allowing for diurnal variation and assuming a balance between production and loss rates of each species integrated over a 24-hour period, for the latitude and temperature of the MkIV observation. Reaction rates and absorption cross sections were adopted from the JPL 97-4 compendium [*DeMore et al.*, 1997], except for the reaction $HNO_3$ + OH. The rate of $HNO_3$ + OH was adopted from *Brown et al.* [1999].

### 3.3. Performance of the Measurements

[17] Table 2 shows the vertical resolutions of the balloon-borne measurements used in the present study. These were estimated from the instantaneous field of view of the instrument to be 1.2–1.5 km at 25 km. Since the vertical resolution of the ILAS instrument (~2.5 km at 25 km) is of the same order as the balloon-borne instruments, the influence of the difference in vertical resolutions on this comparison study is negligible.

[18] Table 2 also shows the precision and absolute accuracy of the balloon-borne measurements. The 1-σ precision was estimated primarily from the errors in the spectral fitting and the atmospheric temperature. The 1-σ absolute accuracy of the retrieval profiles was estimated primarily from the errors in the line parameters or the cross section of $NO_2$. It is noted that the error estimates for each instrument were determined independently by each group. They were not performed in a consistent manner and therefore do not represent a consensus or a basis for comparing instrument performance. This is because the method of estimating the error depends on the nature of the measurements (i.e., thermal emission, solar transmission, etc.) as well as on the retrieval technique employed. Consequently, the predominant error sources of error were sometimes different for the different measurements.

### 3.4. Difference in $NO_2$

[19] The ILAS $NO_2$ profiles and coincident balloon-borne $NO_2$ profiles are shown in Figures 1–5. In each figure, the right panel shows the profile of ILAS aerosol extinction coefficients at a wavelength of 780 nm measured simultaneously with $NO_2$. The left panel is for the comparison of $NO_2$ profiles. For comparisons with MIPAS-B2 and MkIV, the profiles with and without the correction for SZA

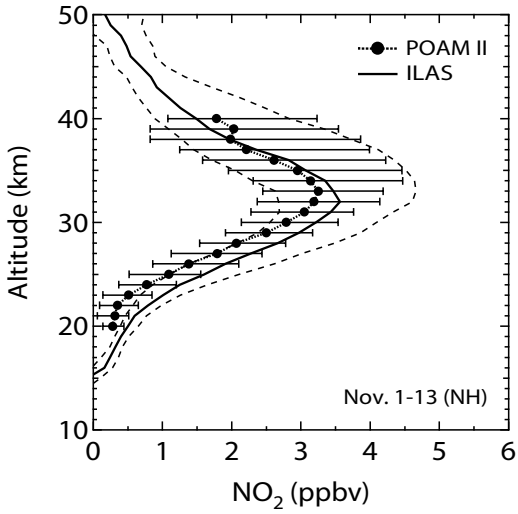


**Figure 6.** Comparison with the POAM II $NO_2$ measurements during 1–13 November in NH. The ILAS median $NO_2$ profile is shown with the solid line. Dashed lines indicate the 67% central values of ILAS $NO_2$. The POAM II median $NO_2$ profile is shown by the dotted line with symbols. Associated bars indicate the 67% central values of POAM II $NO_2$.

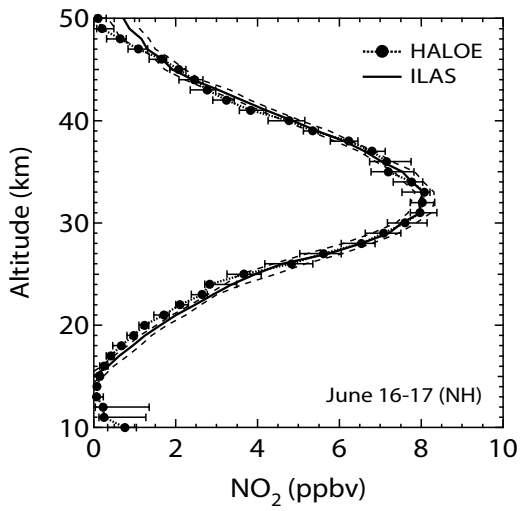


**Figure 7.** Same as Figure 6, but for the comparison with the HALOE $NO_2$ measurements during 16–17 June in NH.

**Table 4.** Time Period, Latitude, and Number of Profiles (*N*) Used for the Comparison of ILAS with POAM II

| Time Period | Latitude | | *N* | |
|---|---|---|---|---|
| | ILAS | POAM II | ILAS | POAM II |
| Nov. 1–13 | 70.2°–67.9°N | 69.2°–67.3°N | 154 | 122 |
| Nov. 1–13 (outside) | 74.8°–70.7°S | 74.1°–70.0°S | 16–87[a] | 11–60[a] |
| Nov. 1–13 (boundary) | 74.8°–70.7°S | 74.1°–70.0°S | 11–37[a] | 8–27[a] |
| Nov. 1–13 (inside) | 74.8°–70.7°S | 74.1°–70.0°S | 34–111[a] | 15–60[a] |

Measurements in the vortex boundary and inside and outside the vortex are denoted by "boundary," "inside," and "outside," respectively.
[a]The number of profiles depends on the altitude, due to the vortex condition at each altitude.

by the model are denoted as "sunset" and "original," respectively.

[20] The comparisons are made only for altitudes chosen with the PV criteria as discussed above. The altitudes used for comparisons are listed in Table 3. Table 3 also shows the altitudes where the $|\Delta NO_2|$ values are greater than 0.5 ppbv (~absolute error in retrieving the ILAS $NO_2$ during the winter), where $\Delta NO_2$ is defined as $NO_2$ (ILAS) − $NO_2$ (correlative measurement).

[21] Some $NO_2$ mixing ratios measured by ILAS at 18–37 km were larger than the balloon measurements by 0.5–0.8 ppbv (Table 3). However, the ILAS $NO_2$ values at 19–21 km on 24 February were negative (Figure 2) and much smaller than those by SAOZ (Table 3).

[22] ILAS aerosol extinction coefficients indicate that optically thick aerosols (most likely PSC particles) were present at 16–25 km and centered at 19–20 km (Figure 2). Since aerosols have a continuous absorption that overlaps the infrared wavelength region for retrieving ILAS $NO_2$ mixing ratios [*Yokota et al.*, 2002], the retrieval algorithm must separate the contribution of aerosols from the total transmittance. The simulations with climatological $NO_2$ profiles and the theoretical extinction spectra, however, show the optically thick aerosols cause the apparent artificial reduction in ILAS $NO_2$ values because of the inadequate correction of aerosol effects employed in the operational data processing [*Yokota et al.*, 2002]. Consequently, the reduction in $NO_2$ at 19–21 km (Table 3) is attributed to interference from the optically thick aerosols, with extinction greater than 0.001 $km^{-1}$ (Figure 2).

## 4. Comparisons With Satellite Measurements

### 4.1. Approach

[23] The ILAS $NO_2$ measurements are compared with 2 satellite solar occultation measurements: (1) the Polar Ozone and Aerosol Measurement (POAM) II in NH and SH during 1–13 November 1996 and (2) the Halogen Occultation Experiment (HALOE) in SH on 24 November, 15–16 December 1996 and 18–19 February 1997, and in NH on 25–31 March and 16–17 June 1997. For each period, these measurements were performed at locations within 1000 km in distance and 1° in latitude of the ILAS measurement points.

[24] For each altitude during winter and early spring, the daily PV values delineating the equatorward and poleward edges of the vortex boundary region are calculated from the maximum convex and concave curvature in the PV values plotted against equivalent latitude, following the method described by *Nash et al.* [1996]. On the basis of this calculation, $NO_2$ data at each altitude are classified as inside the vortex, vortex boundary region, and outside the vortex. This classification is made for data obtained at altitudes below 40 km, where the UKMO data are available.

[25] Median profiles for the $NO_2$ mixing ratios measured by ILAS, POAM II, and HALOE in each period and vortex condition are compared. For each comparison, the 67% central values of the median $NO_2$ mixing ratios measured by ILAS agree with those by POAM II and HALOE measurements to within 10% at 20–40 and 15–45 km, respectively (e.g., Figures 6 and 7), indicating the comparisons of median profiles are valid.

### 4.2. $NO_2$ Profiling by Satellite Measurements

#### 4.2.1. POAM II

[26] The POAM II instrument was launched into a 98.7°-inclination orbit on board the French SPOT-3 satellite on 26 September 1993. POAM II made measurements using solar occultation with nine channels between 353 and 1060 nm until the middle of November 1996. The $NO_2$ value is derived from the differential signal

**Table 5.** Time Period, Latitude, and Number of Profiles (*N*) Used for the Comparison of ILAS with HALOE

| Time Period | Latitude | | *N* | |
|---|---|---|---|---|
| | ILAS | HALOE | ILAS | HALOE |
| Nov. 24 | 67.9°–68.1°S | 68.4–68.9°S | 7 | 11 |
| Dec. 15–16 | 64.4°–64.6°S | 63.9°–65.5°S | 16 | 18 |
| Feb. 18–19 | 75.0°–75.8°S | 74.6°–76.1°S | 24 | 18 |
| March 25–31 (40–50 km) | 68.1°–68.8°N | 67.2°–69.1°N | 92 | 90 |
| March 25–31 (outside) | 68.1°–68.8°N | 67.2°–69.1°N | 14–27[a] | 14–29[a] |
| March 25–31 (boundary) | 68.1°–68.8°N | 67.2°–69.1°N | 7–32[a] | 6–33[a] |
| March 25–31 (inside) | 68.1°–68.8°N | 67.2°–69.1°N | 19–73[a] | 28–89[a] |
| June 16–17 | 56.9°–57.0°N | 56.1°–57.7°N | 23 | 11 |

Measurements in the vortex boundary and inside and outside the vortex are denoted by "boundary," "inside," and "outside," respectively.
[a]The number of profiles depends on the altitude, due to the vortex condition at each altitude.

**Table 6.** Altitudes with $|\Delta NO_2| > 0.5$ ppbv for POAM II Measurements

| Period | ILAS > POAM II | ILAS < POAM II |
|---|---|---|
| Nov. 1–13 (NH) | 23, 25–26, and 28 km | – |
| Nov. 1–13 (SH, outside) | 20–29 and 31 km | – |
| Nov. 1–13 (SH, boundary) | 20, 23–26, 28–29, and 31–32 km | 38 km |
| Nov. 1–13 (SH, inside) | 21–22 km | 36–37 km |

Measurements in the vortex boundary and inside and outside the vortex are denoted by "boundary," "inside," and "outside," respectively.

between two narrow-band channels at 442 and 448 nm. The retrieval altitude ranged between ~20 and 40 km. The ILAS $NO_2$ profiles are compared with those by POAM II (version 6) for 1–13 November 1996 in NH and SH as listed in Table 4.

#### 4.2.2. HALOE

[27] The HALOE instrument was launched on board the Upper Atmosphere Research Satellite (UARS) on 12 September 1991. Routine HALOE observations started on 11 October 1991. Vertical profiles of $NO_2$ and several other trace species are derived using the solar occultation technique. Fifteen vertical profiles in each hemisphere are obtained each day. The ILAS $NO_2$ profiles are compared with those by HALOE (version 19) for five time periods: (1) 24 November, (2) 15–16 December 1996, (3) 18–19 February 1997 in SH, (4) 25–31 March, and (5) 16–17 June 1997 in NH (Table 5).

#### 4.2.3. Difference in $NO_2$

[28] Figures 6 and 7 show representative comparisons of the ILAS $NO_2$ median profiles with those by POAM II (1–13 November in NH) and HALOE (16–17 June in NH), respectively. Table 6 shows the altitudes where the $|\Delta NO_2|$ values for the POAM II are greater than 0.5 ppbv for each comparison. Some ILAS $NO_2$ mixing ratios below 32 km are greater than the POAM II $NO_2$ by >0.5 ppbv, whereas some ILAS $NO_2$ mixing ratios above 36 km are smaller than the POAM II $NO_2$ by >0.5 ppbv.

[29] Table 7 shows the altitudes where the $|\Delta NO_2|$ values for HALOE are greater than 0.5 ppbv for each comparison. Some ILAS $NO_2$ mixing ratios above 37 km are greater than HALOE $NO_2$ by >0.5 ppbv, whereas some ILAS $NO_2$ mixing ratios below 13 km and 29–31 km are smaller than HALOE $NO_2$ by >0.5 ppbv. At 14–26 km, the ILAS $NO_2$ mixing ratios are sometimes larger or smaller than HALOE $NO_2$ values by 0.5 ppbv.

[30] The $\Delta NO_2$ values outside the vortex are compared with those inside the vortex for the POAM II and HALOE data. In Table 8, for each correlative measurement, the $\Delta NO_2$ values averaged in every 5-km layer are shown for inside and outside the vortex. Also shown are the $\delta NO_2$ values defined as the $\Delta NO_2$ divided by the $NO_2$ mixing ratios measured by a correlative measurement. For POAM II data, the $\Delta NO_2$ values outside the Antarctic vortex are 0.9 ppbv (23%) and 0.5 ppbv (7%) at 25 and 30 km, respectively. The $\Delta NO_2$ values outside the vortex are 0.5 ppbv (6%) larger than those inside the vortex at 25 and 30 km. For HALOE data, similarly, the $\Delta NO_2$ values outside the Arctic vortex are <0.3 ppbv (3%) larger than those inside the vortex at 20 and 25 km, and smaller by <0.3 ppbv (7%) at 30 and 35 km. Considering that the estimated error of the ILAS $NO_2$ measurements is 0.5–1.5 ppbv (20%) at 20–30 km, as discussed in section 2, however, the differences in the $\Delta NO_2$ and $\delta NO_2$ values between inside and outside the vortex are within the uncertainty of the ILAS measurements. Table 8 also shows the $\Delta NO_2$ and $\delta NO_2$ values of HALOE data in NH and SH for the same season. The differences in the $\Delta NO_2$ and $\delta NO_2$ values between NH and SH are <0.4 ppbv (10%) at 20–45 km, and are within the uncertainty of the measurements.

## 5. Discussion

[31] The $\Delta NO_2$ and $\delta NO_2$ profiles for the comparisons with each balloon-borne and satellite measurement are shown in Figures 8 and 9 respectively. Table 9 shows the average $\delta NO_2$ values in each 5-km layer. For SAOZ data, the $\Delta NO_2$ and $\delta NO_2$ values at each altitude were averaged from comparisons on 24 February and 20 March. In this calculation, the comparison at 16–25 km on 24 February was excluded because of the presence of optically thick aerosols, as discussed above. For the comparisons with profiles observed by MIPAS-B2 and MkIV, the profiles corrected by a model calculation were used. For the HALOE and POAM II measurements, profiles classified as outside the vortex, vortex boundary region, and inside the vortex were used below 40 km. Since the differences in the $\Delta NO_2$ and $\delta NO_2$ values between inside and outside the vortex and between NH

**Table 7.** Altitudes with $|\Delta NO_2| > 0.5$ ppbv for HALOE Measurements

| Period | ILAS > HALOE | ILAS < HALOE |
|---|---|---|
| Nov. 24 (SH) | 39–41 km | 10–14, 19, 24–25, and 29–30 km |
| Dec. 15–16 (SH) | 16–17, 37–38, 41–43, and 48–50 km | 10–12 and 30–31 km |
| Feb. 18–19 (SH) | 14–19, 21, 23–26, 40–43, and 47–50 km | 10–11 km |
| March 25–31 (NH, 40–50 km) | – | – |
| March 25–31 (NH, outside) | 20 and 24 km | 31 km |
| March 25–31 (NH, boundary) | – | – |
| March 25–31 (NH, inside) | – | 12 km |
| 16–17 June (NH) | 24 and 48–50 km | 11–14 km |

Measurements in the vortex boundary and inside and outside the vortex are denoted by "boundary," "inside," and "outside," respectively.

**Table 8.** The Comparison of the $\Delta NO_2$ (ppbv) and $\delta NO_2$ (%) Values Between Outside and Inside the Vortex and Between NH and SH

| Experiment | 20 km | 25 km | 30 km | 35 km | 40 km | 45 km |
|---|---|---|---|---|---|---|
| POAM II[a] (outside) | ... | 0.91 | 0.52 | −0.20 | ... | ... |
| | | 23% | 7% | −3% | | |
| POAM II[a] (inside) | ... | 0.43 | 0.03 | −0.20 | ... | ... |
| | | 17% | 1% | −3% | | |
| HALOE[b] (outside) | 0.45 | 0.29 | −0.36 | −0.04 | ... | ... |
| | (69%)[c] | 10% | −6% | −1% | | |
| HALOE[b] (inside) | 0.19 | 0.18 | −0.09 | 0.18 | ... | ... |
| | (21%)[c] | 7% | −2% | 6% | | |
| HALOE[d] (NH) | 0.32 | 0.19 | 0 | 0 | 0.17 | 0.06 |
| | (27%)[c] | 7% | 0% | 0% | 5% | (4%)[c] |
| HALOE[e] (SH) | 0.24 | 0.07 | −0.43 | 0.32 | 0.53 | 0.33 |
| | (13%)[c] | 3% | −5% | 5% | 15% | (20%)[c] |

Measurements in the vortex boundary and inside and outside the vortex are denoted by "boundary," "inside," and "outside," respectively.
[a] On 1–13 November in SH.
[b] On 25–31 March in NH.
[c] These values are very sensitive to the HALOE $NO_2$ values due to low $NO_2$ mixing ratios.
[d] On 16–17 June in NH.
[e] On 15–16 December in SH.

and SH were within the uncertainty of the ILAS measurements, as discussed above, the $\Delta NO_2$ and $\delta NO_2$ values at each altitude were averaged for POAM II and HALOE data.

[32] Table 10 shows the systematic and random differences in $NO_2$ between the ILAS and balloon-borne measurements. These systematic and random differences are the average and standard deviation of the $\Delta NO_2$ ($\delta NO_2$) values for all comparisons with the balloon-borne $NO_2$ data, except for the comparison with SAOZ at 16–25 km on 24 February.

[33] Random differences in $NO_2$ at 25 and 30 km were estimated to be 0.32 ppbv (9%) and 0.22 ppbv (3%), respectively (Table 10 and Figure 8). Systematic differences in $NO_2$ at 25 and 30 km were estimated to be 0.25 ppbv (6%) and 0.44 ppbv (11%), respectively, within the uncertainty of the balloon measurements (Table 2).

[34] $NO_2$ concentrations vary along the line of sight for occultation measurements because of the changing SZA. *Sen et al.* [1998] have compared $NO_2$ profiles with and without its diurnal correction using MkIV $NO_2$ measurements performed during SS at midlatitudes. The uncorrected $NO_2$ mixing ratio at 20 km was ~10% higher than the corrected mixing ratio, with progressively smaller differences at higher altitudes. No diurnal correction along the line of sight has been made in ILAS $NO_2$, whereas the correction has been made in HALOE $NO_2$. For 20–25 km, ILAS $NO_2$ is greater than HALOE by 6–27%, with progressively smaller differences at higher altitudes (Table 9 and Figure 9b). This result indicates that the lack of diurnal correction of $NO_2$ accounts for part of the positive bias in ILAS $NO_2$ below 25 km.

[35] Random differences between the ILAS and balloon measurements at 25 and 30 km are as small as 3–9% (Table 10). Furthermore, the $\delta NO_2$ values for HALOE data are within ±10% at 25–40 km (Table 9), suggesting that the lack of diurnal correction is not a significant source of uncertainty above 25 km.

[36] Although the absolute value of random differences between ILAS and balloon-borne measurements at 20 km is as small as 0.3 ppbv (Table 10 and Figure 8a), the percentage value at 20 km is as large as 400% (Table 10 and Figure 8b). The $\delta NO_2$ values for SAOZ and MkIV data at 20 km are smaller than those for LPMA and MIPAS-B2 (Table 9). $NO_2$ values at 20 km measured by SAOZ and MkIV were greater than 1.0 ppbv (Figures 3 and 5), whereas those measured by LPMA and MIPAS-B2 were smaller than 1.0 ppbv (Figures 1 and 4). On the other hand, for HALOE data, the $\delta NO_2$ value at 45 km, where the $NO_2$ concentration is often lower than 1–2 ppbv, is larger than at 25–40 km (Table 9). At 45 km, the standard deviation of the $\delta NO_2$ values is as large as 100% (Table 9). Therefore, the ILAS $NO_2$ measurements below 20 km and above 45 km were most likely degraded by low (<1.0 ppbv) $NO_2$ concentrations.

[37] The $\delta NO_2$ values for the POAM II data at 30–35 km are within ±10%, with progressively larger $\delta NO_2$ at lower altitudes (Table 9 and Figure 9b). This result is very similar to that obtained by *Danilin et al.* [2002], who have compared the ILAS $NO_2$ data with those measured by POAM II in SH in November 1996 using the trajectory hunting technique with large statistics. The $\delta NO_2$ value for POAM II data is 28% at 25 km, where the $\delta NO_2$ is 6% for HALOE. Using the ILAS $NO_2$ data as a reference, the difference of POAM II data from HALOE at 25 km was calculated to be −17%. On the other hand, *Randall et al.* [1998] have made the direct comparisons of $NO_2$ profiles measured by POAM II and HALOE. These comparisons indicate that POAM II data are 5–15% smaller than HALOE at 25 km, accounting for the difference in $\delta NO_2$ values between POAM II and HALOE at 25 km.

## 6. Summary

[38] The results of the comparisons of ILAS $NO_2$ data with those by balloon-borne (LPMA, SAOZ, MIPAS-B2, and MkIV) and satellite (POAM II and HALOE) measurements are summarized in Tables 9 and 10. The best agreement of the ILAS $NO_2$ with the balloon-borne measurements, within ~10%, was obtained at 25–30 km in NH in the winter and spring.

[39] For the comparisons with POAM II measurements in NH and SH in November and HALOE in NH and SH in spring and summer, the $\delta NO_2$ values, defined as (ILAS −

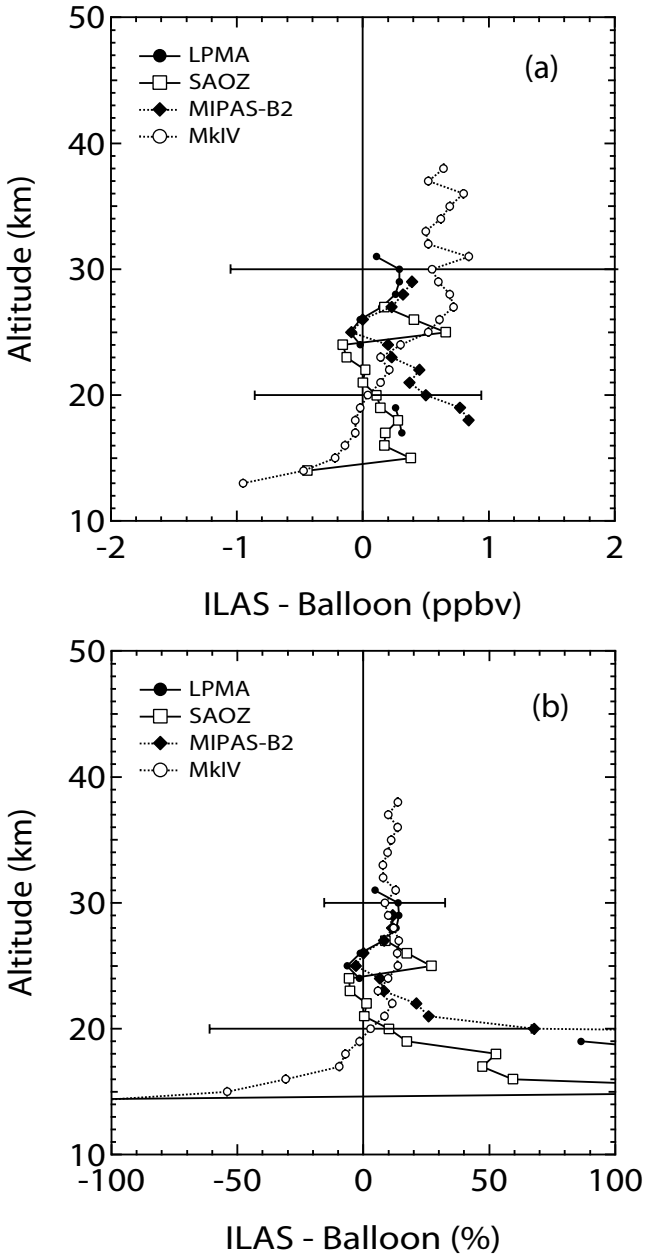


**Figure 8.** (a) The $\Delta NO_2$ and (b) $\delta NO_2$ values for the balloon-borne $NO_2$ mixing ratios as a function of altitude. The values for LPMA, SAOZ, MIPAS-B2, and MkIV are shown by lines with solid circles, squares, diamonds, and open circles, respectively. Error bars indicate the combined uncertainties of the ILAS and balloon measurements, and are shown only for the comparisons with the MkIV profile at 20 and 30 km.

correlative measurement)/(correlative measurement), were calculated for each altitude. Since the differences in the $\delta NO_2$ values between inside and outside the vortex and between NH and SH were within the uncertainty of the ILAS measurements, the averages of all the $\delta NO_2$ values for each altitude were used for the comparisons with POAM II and HALOE data. At 25–40 km, the average $\delta NO_2$ values for HALOE data were within ~±10%. For POAM II data, the $\delta NO_2$ values were within ~±10% at 30–35 km, while the $\delta NO_2$ value at 25 km was 30%. The difference in the $\delta NO_2$ values for HALOE and POAM II data at 25 km is accounted for by the result of the $NO_2$ difference between HALOE and POAM II as described by *Randall et al.* [1998].

[40] The systematic difference between the ILAS and balloon $NO_2$ data was as large as 170% at 20 km, where the $NO_2$ concentrations were lower than 1.0 ppbv. The $\delta NO_2$ values for HALOE data increased to 27% and 40% at 20 and 45 km, respectively, where the $NO_2$ mixing ratios were significantly lower than those at 25–40 km.

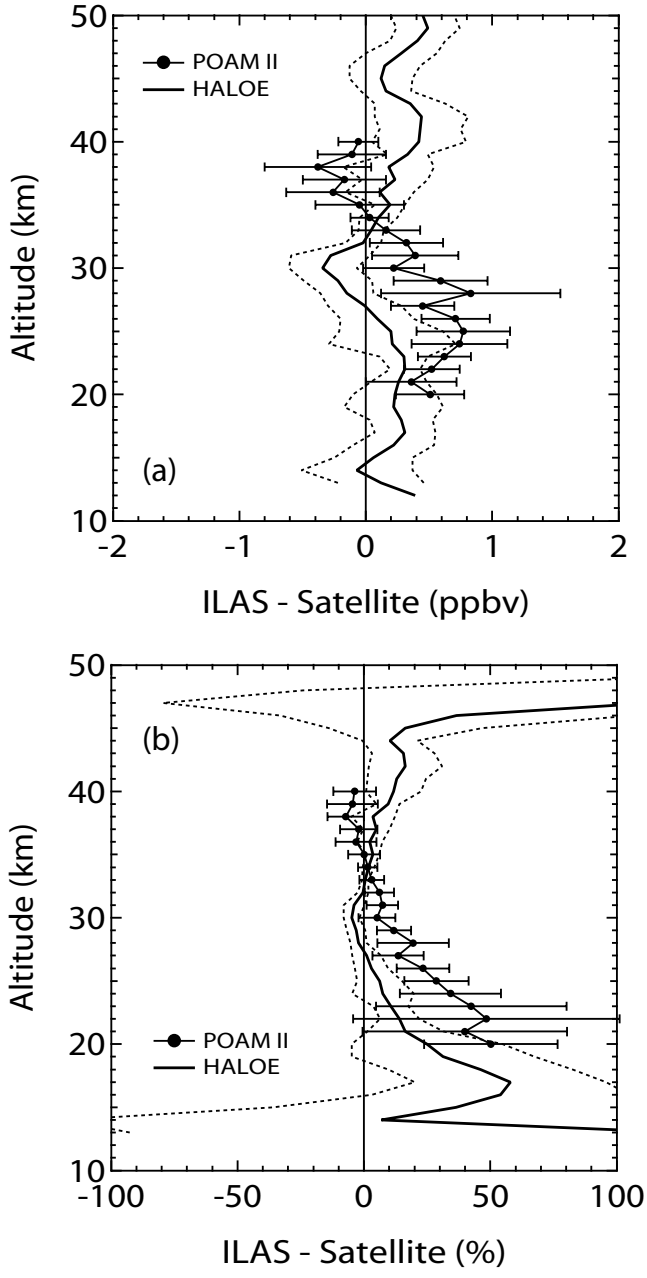


**Figure 9.** (a) $\Delta NO_2$ and (b) $\delta NO_2$ values for POAM II and HALOE $NO_2$ mixing ratios as a function of altitude. Bars and dashed lines indicate 1-σ standard deviations of the values for POAM II and HALOE, respectively.

**Table 9.** The Average $\delta NO_2$ Values in Each 5-km Layer[a]

| Experiment | 15 km | 20 km | 25 km | 30 km | 35 km | 40 km | 45 km |
|---|---|---|---|---|---|---|---|
| LPMA | ... | 155 ± 40 | 0 ± 6 | 11 ± 5 | ... | ... | ... |
| SAOZ | 1 ± 214 | 16 ± 21 | 8 ± 14 | ... | ... | ... | ... |
| MIPAS-B2 | ... | 520 ± 742 | 4 ± 5 | 12 ± 0 | ... | ... | ... |
| MkIV | −99 ± 107 | 3 ± 7 | 11 ± 4 | 10 ± 2 | 10 ± 2 | ... | ... |
| POAM II | ... | ... | 28 ± 21 | 10 ± 9 | 0 ± 6 | ... | ... |
| HALOE | 45 ± 290 | 27 ± 28 | 6 ± 9 | −3 ± 3 | 3 ± 4 | 10 ± 10 | 39 ± 94 |

[a] Average difference ± standard deviation.

[41] Analyses of stratospheric chemistry using ILAS $NO_2$ require the careful consideration of the following effects: (1) negative biases in ILAS $NO_2$ values resulting from interference that was not completely eliminated even with the correction for optically thick PSCs, where aerosol extinction coefficients at 780 nm were greater than 0.001 $km^{-1}$, and (2) the lack of diurnal correction contributing to the positive bias in ILAS $NO_2$ below 25 km.

[42] ILAS version 5.20 $HNO_3$ data achieved excellent agreement (systematic differences $<\pm 0.1$ ppbv) with balloon-borne $HNO_3$ at 20–35 km, as described in the appendix. This indicates small errors in the height registration at these altitudes in the version 5.20 products.

## Appendix A. Validation of ILAS Version 5.20 $HNO_3$ Data

[43] The quality of version 5.20 ILAS $HNO_3$ data is evaluated here in the same way as has been done for the version 3.10 ILAS data by *Koike et al.* [2000]. The $HNO_3$ data used for the comparison with ILAS were obtained from balloon-borne measurements with a chemiluminescence detector, a cold atmospheric emission spectral radiometer, LPMA, MIPAS-B2, a far-infrared spectrometer, and MkIV. At 12 km, the $NO_y$ measurement from the Deutsches Zentrum für Luft-und Raumfahrt Falcon research aircraft is also used. The ILAS $HNO_3$ data used were obtained nearest to the location where the balloon-borne measurements were made. The systematic differences in $HNO_3$ (ILAS minus balloon) were ±15%, −10%, and −19% at 15–25, 30, and 35 km, respectively, for the version 3.10 ILAS data. Random differences were 35%, 10%, and 14–34% at 15, 20–25, and 30–35 km, respectively. It has been suggested that the altitude change in the systematic difference of $HNO_3$ (Figure 10) was caused by an error in the height registration in the version 3.10 ILAS retrieval algorithm [*Koike et al.*, 2000], consistent with the analysis of the version 3.10 ILAS $O_3$ data [*Sasano et al.*, 1999b].

**Table 10.** Systematic and Random $NO_2$ Differences Between the ILAS and Balloon Measurements

| | 20 km | 25 km | 30 km |
|---|---|---|---|
| Systematic difference | | | |
| Percent | 172 | 6 | 11 |
| ppbv | 0.26 | 0.25 | 0.44 |
| Random difference | | | |
| Percent | 439 | 9 | 3 |
| ppbv | 0.26 | 0.32 | 0.22 |

[44] Figure 10 shows the results of comparisons of the version 5.20 $HNO_3$ data with balloon-borne $HNO_3$ measurements. The ILAS version 5.20 $HNO_3$ data achieved excellent agreement (systematic differences $<\pm 0.1$ ppbv) with the balloon-borne $HNO_3$ data in the 20–35 km range (Figure 10). The ILAS $HNO_3$ value at 15 km has a positive bias of ~0.5 ppbv. Systematic differences at 15, 20–25, 30, and 35 km were estimated to be 13%, 0–1%, 4%, and 25%, respectively. The random difference remained unchanged from the algorithm versions 3.10 through 5.20. Most of the altitude change in the systematic difference disappeared (Figure 10), indicating that the error in the height registration has become smaller, especially at 20–25 km.

[45] **Acknowledgments.** The authors thank the French CNES and the SSC Esrange in Kiruna for their excellent balloon operations. We also thank the National Scientific Balloon Facility for the Fairbanks campaign and NASA's Upper Atmosphere Research Program for its support of the U.S. scientists. The PV values of the vortex edges were calculated by G.E. Bodeker at National Institute of Water and Atmospheric Research, New Zealand. The authors wish to thank F.J. Murcray at University of Denver and W.A. Traub at Harvard-Smithsonian Center for providing $HNO_3$ data.

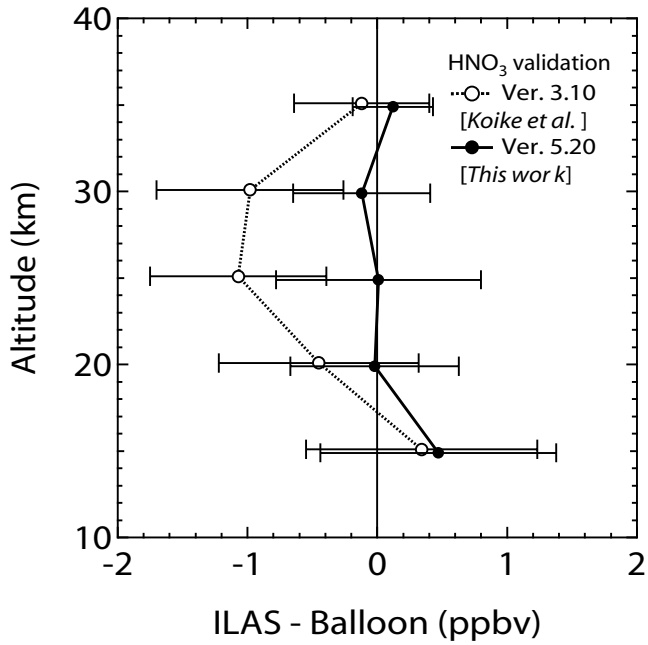


**Figure 10.** Systematic differences between the ILAS and balloon-borne $HNO_3$ mixing ratios for the version 3.10 and 5.20 ILAS data. Bars indicate random differences between ILAS and balloon-borne $HNO_3$ mixing ratios.

## References


Brown, S. S., R. K. Talukdar, and A. R. Ravishankara, Reconsideration of the rate constant for the reaction of hydroxyl radicals with nitric acid, *J. Phys. Chem. A*, *103*, 3031–3037, 1999.

Camy-Peyret, C., Balloon-borne Fourier transform spectroscopy for measurements of atmospheric trace gases, *Spectrochim. Acta, Part A*, *51*, 1143–1152, 1995.

Crutzen, P. J., The influence of nitrogen oxides on the atmospheric ozone content, *Q. J. R. Meteorol. Soc.*, *96*, 320–325, 1970.

Danilin, M. Y., et al., Trajectory hunting as an effective technique to validate multiplatform measurements: Analysis of the MLS, HALOE, SAGE-II, ILAS, and POAM-II data in October–November 1996, *J. Geophys. Res.*, *107*, doi:10.1029/2001JD002012, in press, 2002.

DeMore, W. B., S. P. Sander, D. M. Golden, R. F. Hampton, M. J. Kurylo, C. J. Howard, A. R. Ravishankara, C. E. Kolb, and M. J. Molina, Chemical kinetics and photochemical data for use in stratospheric modeling, *JPL Publ.*, *97-4*, 1997.

Fahey, D. W., et al., Ozone destruction and production rates between spring and autumn in the Arctic stratosphere, *Geophys. Res. Lett.*, *27*, 2605–2608, 2000.

Friedl-Vallon, F., G. Maucher, H. Oelhaf, M. Seefeldner, O. Trieschmann, G. Wetzel, and H. Fischer, The balloon-borne Michelson Interferometer for Passive Atmospheric Sounding (MIPAS-B2)—Instrument and results, in *Optical Spectroscopic Techniques and Instrumentation for Atmospheric and Space Research III, Proceedings of SPIE, 3756*, 9–16, 1999.

Hanson, D., and K. Mauersberger, Laboratory studies of the nitric acid trihydrate: Implications for the south polar stratosphere, *Geophys. Res. Lett.*, *15*, 855–858, 1988.

Jucks, K. W., D. G. Johnson, K. V. Chance, W. A. Traub, R. J. Salawitch, and R. A. Stachnik, Ozone production and loss rate measurements in the middle stratosphere, *J. Geophys. Res.*, *101*, 28,785–28,792, 1996.

Kanzawa, H., C. Camy-Peyret, Y. Kondo, and N. Papineau, Implementation and first scientific results of the ILAS validation balloon campaign at Kiruna-Esrange in February–March 1997, in *Proceedings of 13th ESA Symposium, European Rocket and Balloon Programmes and Related Research*, *Oland, Sweden*, *26–29 May 1997*, *Eur. Space Agency Spec. Publ.*, *ESA-SP-397*, 211–215, 1997.

Koike, M., et al., A comparison of Arctic $HNO_3$ profiles measured by the Improved Limb Atmospheric Spectrometer and balloon-borne sensors, *J. Geophys. Res.*, *105*, 6761–6771, 2000.

Nash, E. R., P. A. Newman, J. E. Rosenfield, and M. R. Schoeberl, An objective determination of the polar vortex using Ertel's potential vorticity, *J. Geophys. Res.*, *101*, 9471–9478, 1996.

Oelhaf, H., et al., Remote sensing of the Arctic stratosphere with the new balloon-borne MIPAS-B2 instrument, in *Proceedings of the 3rd European Workshop 18 to 22 September 1995*, edited by J. A. Pyle et al., Eur. Comm., Brussels, Luxembourg, 270–275, 1996.

Osterman, G. B., R. J. Salawitch, B. Sen, G. C. Toon, R. A. Stachnik, H. M. Pickett, J. J. Margitan, J.-F. Blavier, and D. B. Peterson, Balloon-borne measurements of stratospheric radicals and their precursors: Implications for the production and loss of ozone, *Geophys. Res. Lett*, *24*, 1107–1110, 1997.

Osterman, G. B., B. Sen, G. C. Toon, R. J. Salawitch, J. J. Margitan, J.-F. Blavier, D. W. Fahey, and R. S. Gao, Partitioning of $NO_y$ species in the summer Arctic stratosphere, *Geophys. Res. Lett*, *26*, 1157–1160, 1999.

Payan, S., C. Camy-Peyret, P. Jeseck, T. Hawat, G. Durry, and F. Lefèvre, First direct simultaneous HCl and $ClONO_2$ profile measurements in the Arctic vortex, *Geophys. Res. Lett*, *25*, 2663–2666, 1998.

Pommereau, J.-P., and F. Goutail, $O_3$ and $NO_2$ ground-based measurements by visible spectrometry during Arctic winter and spring 1988, *Geophys. Res. Lett.*, 891–894, 1988.

Randall, C. E., D. W. Rusch, R. M. Bevilacqua, K. W. Hoppel, and J. D. Lumpe, Polar Ozone and Aerosol Measurement (POAM) II stratospheric $NO_2$, 1993–1996, *J. Geophys. Res.*, *103*, 28,361–28,371, 1998.

Reddmann, T., R. Ruhnke, and W. Kouker, Three-dimensional model simulations of $SF_6$ with mesospheric chemistry, *J. Geophys. Res.*, *106*, 14,525–14,537, 2001.

Ruhnke, R., W. Kouker, and T. Reddmann, The influence of the OH + $NO_2$ + M reaction on the $NO_y$ partitioning in the late Arctic winter 1992/1993 as studied with KASIMA, *J. Geophys. Res.*, *104*, 3755–3772, 1999.

Sander, S. P., et al., Chemical kinetics and photochemical data for use in stratospheric modeling, *JPL Publ.*, *00-3*, 2000.

Sasano, Y., M. Suzuki, T. Yokota, and H. Kanzawa, Improved Limb Atmospheric Spectrometer (ILAS) for stratospheric ozone layer measurements by solar occultation technique, *Geophys. Res. Lett.*, *26*, 197–200, 1999a.

Sasano, Y., et al., Validation of ILAS version 3.10 ozone with ozonesonde measurements, *Geophys. Res. Lett.*, *26*, 831–834, 1999b.

Sen, B., G. C. Toon, G. B. Osterman, J.-F. Blavier, J. J. Margitan, R. J. Salawitch, and G. K. Yue, Measurements of reactive nitrogen in the stratosphere, *J. Geophys. Res.*, *103*, 3571–3585, 1998.

Toon, G. C., The JPL MkIV interferometer, *Opt. Photonics News*, *2*, 19–21, 1991.

Vandaele, A. C., C. Hermans, P. C. Simon, M. Carleer, R. Colin, S. Fally, M. F. Merienne, A. Jenouvrier, and B. Coquart, Measurements of the $NO_2$ absorption cross-section from 42 000 $cm^{-1}$ to 10 000 $cm^{-1}$ (238–1000 nm) at 220 K and 294 K, *J. Quant. Spectrosc. Radiat. Transfer*, *59*, 171–184, 1998.

Wetzel, G., et al., $NO_y$ partitioning and budget and its correlation with $N_2O$ in the Arctic vortex and in summer midlatitudes in 1997, *J. Geophys. Res.*, *107*(D16), 4280, doi:10.1029/2001JD000916, 2002.

Yokota, T., et al., Improved Limb Atmospheric Spectrometer (ILAS) data retrieval algorithm for version 5.20 gas profile products, *J. Geophys. Res.*, *107*, doi:10.1029/2001JD000628, in press, 2002.



R. M. Bevilacqua, Naval Research Laboratory, Code 7220, Washington, DC 20375, USA. (bevilacqua@nrl.navy.mil)

C. Camy-Peyret and S. Payan, Laboratoire de Physique Moléculaire et Applications, Université Pierre et Marie Curie, CNRS, 4 place Jussieu, Bte 76, 75252 Paris cedex 05, France. (camy@ccr.jussieu.fr; payan@ccr.jussieu.fr)

M. Y. Danilin, Atmospheric and Environmental Research, Inc., 131 Hartwell Avenue, Lexington, MA USA. (danilin@aer.com)

F. Goutail and J. P. Pommereau, Service d'Aeronomie du CNRS, BP 3, Verrières le Buisson, 91371 France. (florence.goutail@aerov.jussieu.fr; pommereau@aerov.jussieu.fr)

H. Irie, Solar-Terrestrial Environment Laboratory, Nagoya University, 3-13, Honohara, Toyokawa, Aichi, 442-8507, Japan. (irie@stelab.nagoya-u.ac.jp)

H. Kanzawa, H. Nakajima, Y. Sasano, T. Sugita, and T. Yokota, National Institute for Environmental Studies, 16-2, Onogawa, Tsukuba, 305-0053, Japan. (kanzawa@nies.go.jp; hide@nies.go.jp; sasano@nies.go.jp; tsugita@nies.go.jp; yoko@nies.go.jp)

M. Koike, Department of Earth and Planetary Science, Graduate School of Science, University of Tokyo, 7-3-1, Hongo, Bunkyo, Tokyo, 113-0033, Japan. (koike@stelab.nagoya-u.ac.jp)

Y. Kondo, Research Center for Advanced Science and Technology, University of Tokyo, 4-6-1, Komaba, Meguro, Tokyo, 153-8904, Japan. (kondo@atmos.rcast.u-tokyo.ac.jp)

H. Oelhaf and G. Wetzel, Institut für Meteorologie und Klimaforschung, Forschungszentrum Karlsruhe, P.O. Box 3640, D-76021 Karlsruhe, Germany. (hermann.oelhaf@imk.fzk.de; gerald.wetzel@imk.fzk.de)

J. B. Renard, Laboratoire de Physique et Chimie de l'Environnement, CNRS, 3A Avenue de la Recherche Scientifique, F-45071 Orléans cedex 2, France. (jbrenard@cnrs-orleans.fr)

J. M. Russell III, Center for Atmospheric Sciences, 23 Tyler Street, Hampton University, P.O. Box 6075, VA 23668, Hampton, USA. (james.russell@hamptonu.edu)

B. Sen and G. C. Toon, Jet Propulsion Laboratory, California Institute of Technology, M. S. 183–301, 4800 Oak Grove Drive, Pasadena, CA 91109-8099, USA. (sen@mark4sun.jpl.nasa.gov; toon@mark4sun.jpl.nasa.gov)